ACS APPLIED MATERIALS & INTERFACES

Research Article

www.acsami.org

Porous Spherical CaO-based Sorbents via PSS-Assisted Fast Precipitation for CO_2 Capture

Shengping Wang,* Lijing Fan, Chun Li, Yujun Zhao, and Xinbin Ma

Key Laboratory for Green Chemical Technology, School of Chemical Engineering and Technology, Tianjin University; Collaborative Innovation Center of Chemical Science and Engineering, Tianjin 300072, China

ABSTRACT: In this paper, we report the development of synthetic CaO-based sorbents via a fast precipitation method with the assistance of sodium poly(styrenesulfonate) (PSS). The effect of PSS on physical properties of the CaO sorbents and their CO_2 capture performance were investigated. The presence of PSS dispersed the CaO particles effectively as well as increased their specific surface area and pore volume remarkably. The obtained porous spherical structure facilitated CO_2 to diffuse and react with inner CaO effectively, resulting in a significant improvement in initial CO_2 carbonation capacity. A proper amount of Mg^{2+} precursor solution was doped during a fast precipitation process to gain CaO-based sorbents with a high anti-sintering property, which maintained the porous spherical structure with the high specific surface area. CaO-based sorbents derived from a $Mg_xCa_{1-x}CO_3$ precursor existed in the form of CaO and MgO. The homogeneous distribution of MgO in the CaO-based sorbents effectively prevented the CaO crystallite from growing and sintering, further resulting in the favorable long-term durability with carbonation capacity of about 52.0% after 30 carbonation/calcination cycles.

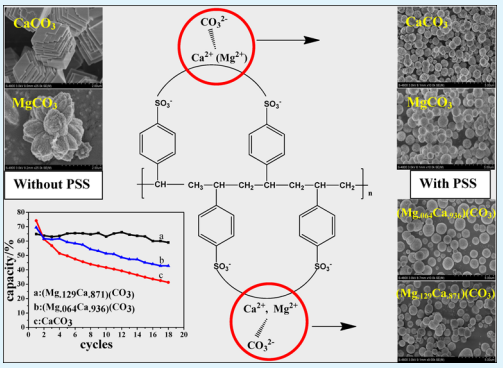

KEYWORDS: *CO_2 capture, porous spherical structure, fast precipitation method, $Mg_xCa_{1-x}CO_3$*

INTRODUCTION

As a promising postcombustion CO_2 capture technology, CaO-based sorbents have recently drawn increasing attention to restrain CO_2 anthropogenic emissions from power plants fired with fossil fuels.[1−4] Compared with other sorbents for CO_2 capture, i.e., amine,[5,6] zeolite, carbon-based materials,[7] and hydrotalcite-like compounds,[8] CaO-based sorbents show great potential due to the following advantages: high initial adsorption capacity (0.786 g CO_2/g CaO),[9,10] fast CO_2 carbonation/decarbonation kinetics, low cost of the naturally occurring precursor (i.e., limestone), and its wide availablility.[11] The CO_2 capture process with CaO-based sorbents contains carbonation and calcination periods, and during the carbonation stage, CaO captures CO_2 and transfers to $CaCO_3$. Due to the formation of $CaCO_3$ with larger molar volumes (36.9 cm^3 mol^{-1}) than CaO (16.7 cm^3 mol^{-1}), the sorbents experience pore blockage, obtaining a dense product layer that prevents the diffusion of CO_2 and causes part of CaO nonreactive.[2,10,12] Additionally, the sintering of calcium-based sorbents at high temperatures is considered as the major cause of loss-in-capacity, supported by observations of morphological and structural changes in CaO sorbents after multiple cycles. This phenomenon is attributed to the lower Tammann temperature of $CaCO_3$ than the temperature employed for carbonation and calcination.

Correspondingly, the addition of an inert material with a high melting point is adopted to improve the thermal stability of sorbent during the multicycle carbonation/calcination process.[13] Sorbents with a high antisintering property were synthesized through the method of doping with inert materials, such as Al_2O_3,[14] $CaZrO_3$,[15] TiO_2,[16] and MgO[17] with a high melting point, via a physical method or chemical synthesis. Moreover, in order to gain sorbents with a higher carbonation conversion, several strategies have been used to enhance the reactivity of sorbents, including CaO modified with an ethanol/water solution,[18,19] treated with organic acids,[20,21] prepared from a novel preparation method such as sol−gel derived,[22,23] spray-drying technique[24] and mechanical activation,[25] and fabricating with the assitance of surfactant.[10,26,27] From the perspective of modified material structure, the above methods yield materials with higher reactivity and capacity by improved specific surface area and total pore volume.

On the other hand, the merely controlled synthesis of $CaCO_3$ materials has attracted much attention in the materials science field, and a wide variety of novel $CaCO_3$ structures, including $CaCO_3$ porous spheres, honeycombs, rodlike particles, hexagonal plates, and multibranched hierarchical structures have been synthesized employing biomimetic self-assembly mechanisms or with the assistance of organic additives and/or templates.[28−30] Among these special structures, in the presence of poly(styrenesulfonate) (PSS), the porous spherical $CaCO_3$ was obtained with higher specific surface area and total pore volume,[31] which provide the possibility of favoring the diffusion of CO_2 to the inner CaO

Received: July 26, 2014
Accepted: September 24, 2014
Published: September 24, 2014

when it was used for CO_2 capture. However, this kind of porous spherical $CaCO_3$ has not been applied to high temperature CO_2 capture.

This work is concernd with the preparation and characterization of a novel, porous sphere structured CaO-based sorbent with a higher specific surface area and total pore volume, which were prepared by a fast precipitation method in the presence of a simple polymer, PSS.[32] To gain sorbents with excellent stability, Mg^{2+} was coprecipitated with Ca^{2+} during the fast precipitation process. These novel CaO-based sorbents were applied for CO_2 capture and the carbonation capacity and durability was tested. The effects of PSS and inert material contents on the structure and CO_2 capture performance of CaO-based sorbents were also investigated.

EXPERIMENTAL SECTION

Materials and Sorbents Preparation. $CaCO_3$ samples were synthesized via a fast precipitation method in the presence of sodium poly(styrenesulfonate) (J&K Scientific, MW ≈ 70 000) at 25 °C in aqueous solutions. The stock solutions of $CaCl_2$ (Tianjin Kelmel, 99.9%) and Na_2CO_3 (Tianjin Kelmel, 99.9%) both at a concentration of 4 mM were prepared first. PSS was dissolved in solutions with its concentration of 1 g/L. In a typical synthesis, 100 mL of $CaCl_2$ and 0.2 g of PSS were added in a 500 mL three-necked, round-bottomed flask under vigorous stirring for 30 min. Then 100 mL of Na_2CO_3 solution was injected quickly into the above mixed solution. The resultant mixture was continuously stirred for another 15 min, after which the products were collected by centrifugation, washed with deionized water several times, and dried at 90 °C overnight.[31] The Ca^{2+}/Mg^{2+} coprecipitation samples were prepared in the same way just substituting the above $CaCl_2$ solution with $CaCl_2$ and $MgCl_2$ mixing solution with a certain Ca^{2+}/Mg^{2+} proportion. All sorbent precursors were calcined at 700 °C in a N_2 atmosphere for 30 min to allow sufficient decomposition of the calcium carbonate precursors.

Sorbents Testing. The cyclic carbonation/calcination performance of the Cao-based sorbents was investigated using thermogravimetric analysis (TGA, NETZSCH STA 449F3) with the precision of 10^{-6} g. In a standard test, approximately 10 mg of $CaCO_3$ or $CaCO_3$-based precursor was placed in a quartz sample pan and heated to a calcination temperature of 700 °C at a rate of 10 °C/min under N_2 atmosphere at atmospheric pressure and maintained for 30 min for complete calcination. Carbonation was initiated when the temperature was dropped to 650 °C. Once the carbonation temperature was reached, the carbonation proceeded for 45 min in 50% CO_2 balanced by N_2. After carbonation, a pure N_2 flow was introduced into the thermogravimetric analyzer for 30 min instead of CO_2 for calcination at 700 °C. The above carbonation/calcination process was repeated for 18 cycles and the corresponding multicycle results were obtained. The carbonation capacity of the sorbent in TGA tests were calculated on the basis of mass change in the following equation:

$$\text{carbonation capacity (\%)} = \frac{\text{mass of adsorbed } CO_2}{\text{mass of the sorbent}} \times 100\%$$

Characterization. The surface morphology and the EDS-mapping of samples were obtained using scanning electron microscopy (SEM) with a Hitachi S4800 field-emission microscope at 10.0 kV. The powder samples were sprayed with gold for 60 s to ensure conductivity.

Porosity characterization was determined from N_2 adsorption and desorption isotherms on a Micromeritics Tristar volumetric adsorption analyzer, measured with N_2 at −196 °C. The surface area was gained from the Brunauer−Emmett−Teller (BET) equations. The total pore volume was measured at the relative pressure (P/P_0) of 0.995 and the pore size distribution measurement was determined using the Barrett−Joyner−Halenda (BJH) method.

Quantitative X-ray diffraction (XRD) analysis for the uncalcined and calcined powders was conducted on a Rigaku D/max-2500 diffractometer to identify crystal phases operating in a 2θ range of 10−90° with a scanning rate of 8°/min.

RESULTS AND DISCUSSION

Effect of PSS on the Structure, Morphology and CO_2 Capture of $CaCO_3$. The phase compositions of the as-synthesized calcium carbonate with and without PSS are displayed in Figure 1. As presented in the XRD patterns, all the

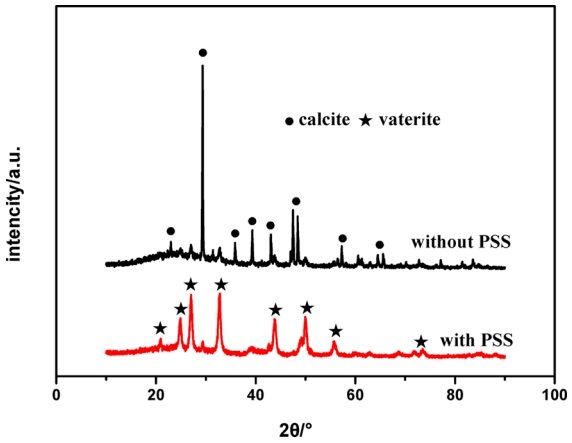

Figure 1. XRD patterns of $CaCO_3$ prepared with or without PSS.

peaks can be indexed as the calcite structure (JCPDS #83-0578) in the absence of PSS, indicating a pure calcite phase is obtained for the corresponding product. A pure vaterite phase (JCPDS #74-1867) was obtained instead of the calcite phase with the addition of PSS, meaning that PSS can exert significant influence on the phase formation of the synthesized calcium carbonate. The polymorph of the synthesized calcium carbonate products transforms from pure calcite in PSS-free reactions into vaterite in PSS-containing reactions. Such a phase selection can be rationalized from the following two aspects: (1) decrease of driving force by reducing the interfacial energy and (2) phase stabilization effect caused by the adsorbed PSS.[31]

The SEM images of $CaCO_3$ prepared with or without PSS are presented in Figure 2. As shown in Figure 2a,b, in the presence of PSS, it is noted that $CaCO_3$ particles were a porous sphere shape and uniform in size (approximately 500−800 nm). The presence of PSS prevented the agglomeration of $CaCO_3$ particles and produced the porous sphere structure effectively. In the process of $CaCO_3$ crystal growth, the release rate of Ca^{2+} and CO_3^{2-} was the key to the formation of $CaCO_3$. In the presence of PSS, Ca^{2+} with positive charge in aqueous solution can be absorbed onto the negatively charged sulfonic acid groups on the huge molecular chain to form the chelate, and then the chelate released Ca^{2+} slowly to precipitate with CO_3^{2-}, thus delaying the precipitation process and further forming the uniform precipitation particles. The macromolecular chain sulfonic acid group of PSS had very strong dispersion effect, which dispersed tiny $CaCO_3$ particles suspended in the solution. Furthermore, in the process of $CaCO_3$ grain formation, due to the three-dimensional reticular structure of PSS, CO_3^{2-} in the solution adsorbed on the polymer long chain from different directions and combined with the released Ca^{2+} to form $CaCO_3$ crystal nucleus, which made it easier to grow up to form porous sphere. Also, the decrease of interfacial energy by adding PSS further favored the formation of sphere structure.[31,33,34] Thus, with the assistance

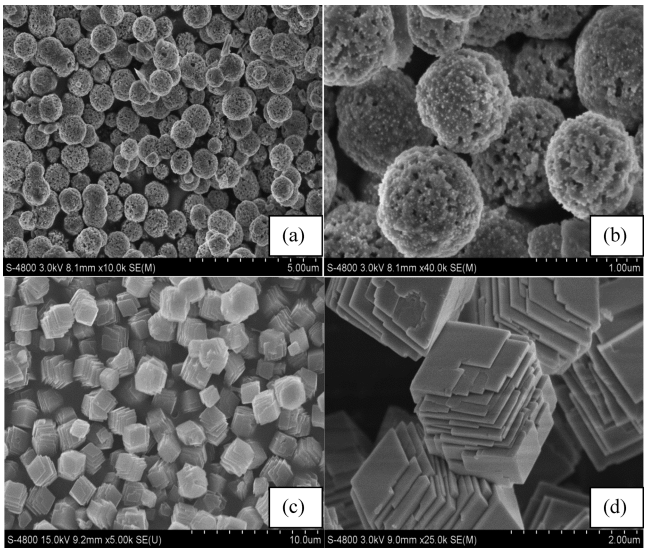

Figure 2. SEM images of $CaCO_3$ precipitation (a, b) with PSS and (c, d) without PSS.

of PSS, porous spherical $CaCO_3$ with better dispersion and smaller particle size could be gained.

Comparatively, as shown in Figure 2c,d, the $CaCO_3$ precipitation obtained without adding PSS, merely precipitating Ca^{2+} and CO_3^{2-}, showed a dense and plate-like morphology particles like a cube with size about 1 μm due to the fast and intensive precipitation of $CaCO_3$. In this case, the nanosized platelets stacked up to form particles of several micrometer sizes, likely due to subsequent ripening in solution. Moreover, its surface appeared smooth and compact and these large agglomerates were not a porous structure. Thus, the addition of PSS exerted much influence on the $CaCO_3$ morphology, facilitating the formation of the porous sphere structure.

Textural properties including specific surface area and pore volume of the obtained $CaCO_3$ were also determined using nitrogen sorption technique. Figure 3a shows the adsorption/desorption isotherms of $CaCO_3$ precipitation with PSS. The specific surface area and pore volume of $CaCO_3$ prepared with PSS were 110.5 m^2/g and 0.122 cm^3/g, respectively. The higher specific surface area and pore volume were attributed to the smaller void generated in the porous structure of the sorbents.

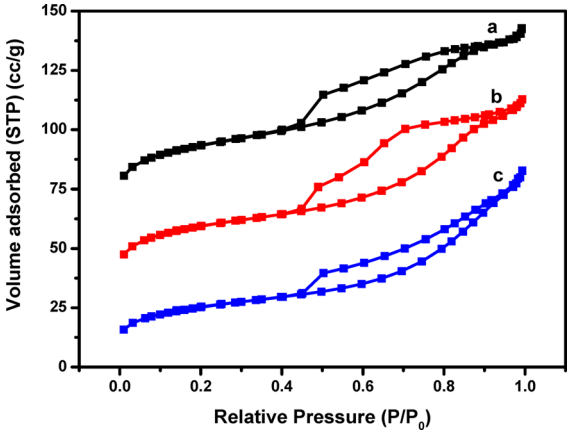

Figure 3. N_2 adsorption/desorption isotherms of (a) $CaCO_3$ precipitation with PSS, (b) $Mg_{.129}Ca_{.871}CO_3$, and (c) $Mg_{.064}Ca_{.936}CO_3$.

The carbonation capacities of CaO derived from $CaCO_3$ prepared with PSS (annotated as CaO-P), without PSS (annotated as CaO) and commercial $CaCO_3$ (annotated as CaO-CC) are shown in Figure 4. The comparison of the initial

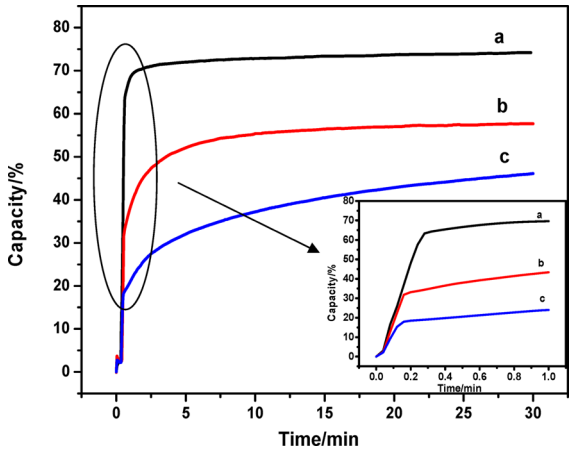

Figure 4. Initial capacity comparison of three sorbents derived from different precursors (a) CaO-P, (b) CaO−CC, and (c) CaO. Carbonation: 650 °C, 45 min, 50% CO_2 in N_2. Calcination: 700 °C, 30 min, pure N_2.

capacity of the sorbents was found to be as follows: CaO-P (74.2%) > CaO-CC (57.7%) > CaO (46.6%). It is worth noting that for CaO-P sorbent, a significant improvement in initial CO_2 carbonation capacity was achieved, which is attributed to the porous sphere structure with higher surface area and pore volume. It can be seen that the carbonation of the sorbents occurs in two stages: an initial fast reaction controlled phase (0−0.3 min) and a slower diffusion controlled phase (0.3−30 min). Table 1 presented the capacity comparison of the three

Table 1. Capacity Comparison of the Sorbents

	total capacity (%)	capacity in fast reaction period (%)	capacity in fast reaction period/total capacity (%)
CaO-P	74.2	63.4	85.4
CaO-CC	57.7	31.8	55.1
CaO	46.0	17.9	38.9

sorbents in the different carbonation period. From Table 1, it was indicated that most of the capacity was acquired for CaO-P sorbent in the first reaction period, taking up 85.4% of the whole carbonation capacity, which was benefited by the porous structure of the sorbent. The abundant pores facilitated the diffusion of CO_2 and further promoted the reaction between CO_2 and the inner CaO.

As for a suitable CO_2 sorbent, the resistance to thermal sintering has to be taken into consideration for a multiple carbonation/calcination cycles test. The long-term capacity of CaO-P and CaO-CC is shown in Figure 5. It is noted that both the sorbents experienced rapid decays in capacity with carbonation/calcination cycles. The carbonation capacity of CaO-P decreased from 72.5% to 31.3% after 18 cycles, which was attributed to $CaCO_3$ sintering because of its lower Tammann temperature (561 °C) compared with the carbonation (650 °C) and calcination (700 °C) temperatures. Meanwhile, it was found that a higher capacity of each cycle of

dx.doi.org/10.1021/am5049527 | ACS Appl. Mater. Interfaces 2014, 6, 18072−18077

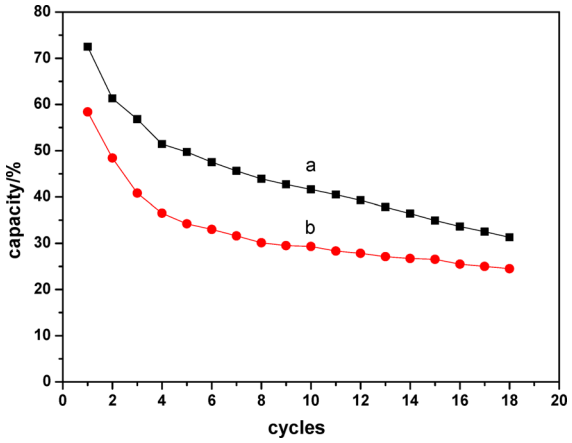

Figure 5. Carbonation capacity vs cycles for sorbents (a) CaO-P and (b) CaO-CC. Carbonation: 650 °C, 45 min, 50% CO_2 in N_2. Calcination: 700 °C, 30 min, pure N_2.

CaO-P for CO_2 capture was obtained compared with CaO-CC. The possible reason may be that the structure of CaO-P sorbents facilitated the diffusion of CO_2 and reaction with the inner CaO, resulting in a higher capacity of each cycle.

Effect of Inert MgO on the Structure, Morphology and CO_2 Capture of CaO-based Sorbents. Because $CaCO_3$ sintering leads to the loss of capacity with cycles, Mg^{2+} precursor solutions with the different contents were introduced during the fast precipitation process to gain sorbents with favorable stability. The XRD patterns of the synthetic sorbent precursors and sorbents after calcination are displayed in Figures 6 and 7, respectively. As shown in Figure 6, the sorbent

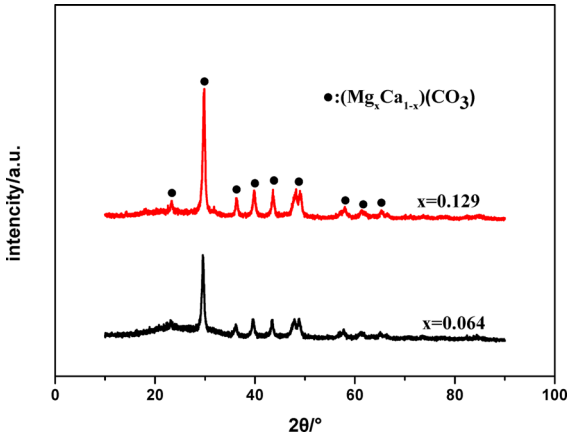

Figure 6. XRD patterns of $(Mg_xCa_{1-x})(CO_3)$ with different proportions of *x*.

precursors with the different Ca^{2+}/Mg^{2+} proportion existed in the form of $Mg_xCa_{1-x}CO_3$, showing that Mg^{2+} and Ca^{2+} mixed well. The crystal form of $(Mg_{.064}Ca_{.936})(CO_3)$ (JCPDS #86-2335) and $(Mg_{.129}Ca_{.871})(CO_3)$ (JCPDS #86-2336) were obtained with Ca^{2+}/Mg^{2+} proportions of 4:1 and 2:1, respectively. Figure 7 shows the XRD results of the final sorbents derived from Ca and Mg compound with the different Ca^{2+}/Mg^{2+} proportion after calcination. All the diffraction peaks indexed that the sorbents were in the form of CaO and MgO. Moreover, the grain size of CaO decreased with the addition of MgO according to the results calculated by the Scherrer equation. The grain size of pure CaO was 86.0 nm

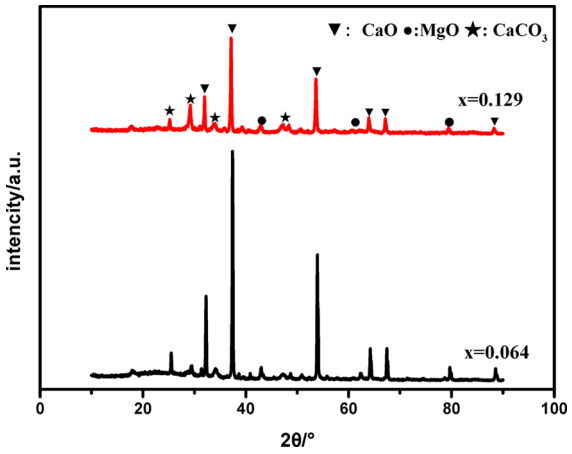

Figure 7. XRD patterns of CaO-MgO sorbents derived from $(Mg_xCa_{1-x})(CO_3)$ with different proportions of *x*.

whereas that of CaO derived from $(Mg_{.064}Ca_{.936})(CO_3)$ and $(Mg_{.129}Ca_{.871})(CO_3)$ was 46.3 and 32.2 nm, respectively, indicating that the addition of MgO prevented the particle growth of CaO. The CaO-based sorbent derived from $(Mg_{.129}Ca_{.871})(CO_3)$ possessed more inert MgO, ensuring its higher anti-sintering property for CO_2 capture.

The SEM images of $(Mg_{.064}Ca_{.936})(CO_3)$ and $(Mg_{.129}Ca_{.871})$-(CO_3) are shown in Figure 8. It is surprisingly noted that,

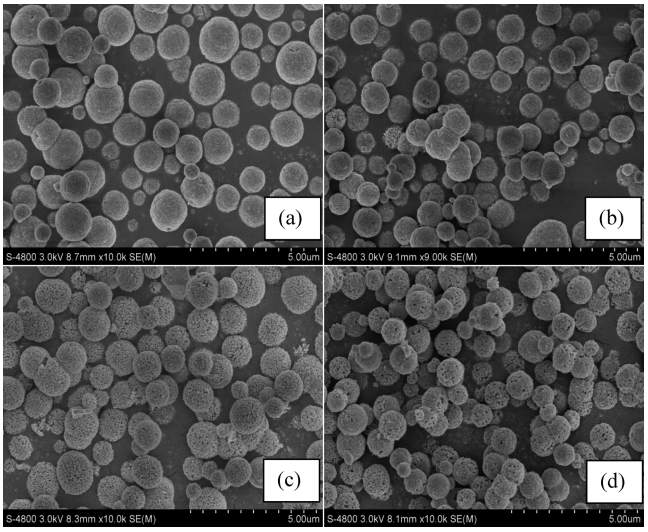

Figure 8. SEM images of sorbents (a) $(Mg_{.064}Ca_{.936})(CO_3)$, (b) $(Mg_{.129}Ca_{.871})(CO_3)$, (c) derived from $(Mg_{.064}Ca_{.936})(CO_3)$, and (d) derived from $(Mg_{.129}Ca_{.871})(CO_3)$.

similar to pure $CaCO_3$ prepared with PSS, the Mg and Ca compound emerged as a porous sphere structure about 800−1200 nm in size, which was distributed dispersedly. Interestingly, the spheres kept intact in morphology and the porous structure was still unchanged after calcination, showing that the porous sphere structure of the sorbents was very stable. Comparatively, Figure 9 displayed the SEM images of precipitation of $MgCO_3$ with or without the addition of PSS. It was found that the structure of $MgCO_3$ was also the porous sphere with its size of about 800−1200 nm in the presence of PSS, whereas $MgCO_3$ precipitation presented a "flower" morphology without PSS, showing that PSS had the same effect on $MgCO_3$ precipitation as that of $CaCO_3$. This

dx.doi.org/10.1021/am5049527 | ACS Appl. Mater. Interfaces 2014, 6, 18072−18077

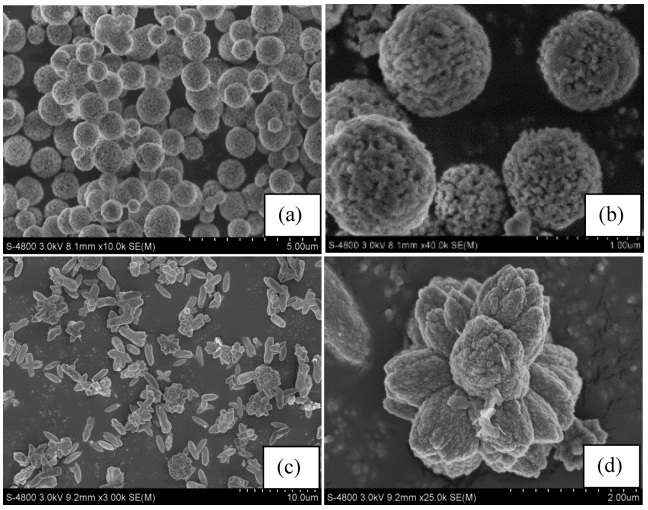

Figure 9. SEM images of $MgCO_3$ precipitation (a, b) with PSS and (c, d) without PSS.

phenomenon may illustrate the compound $Mg_xCa_{1-x}CO_3$ from precipitating Ca^{2+} and Mg^{2+} simultaneously in the presence of PSS was in the form of a porous sphere structure.

The images of the EDS mapping of sorbent derived from $Mg_{.129}Ca_{.871}CO_3$ are presented in Figure 10. From Figure 10, it

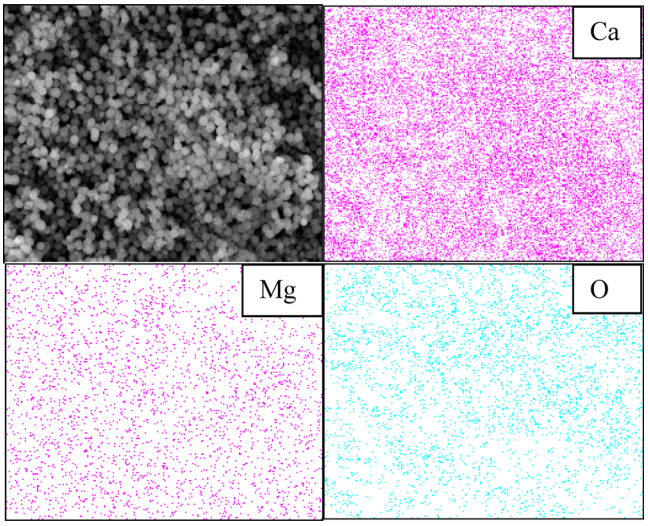

Figure 10. EDS mapping of porous sphere sorbent of CaO-MgO.

was demonstrated that both Ca and Mg were distributed quite uniformly over the sphere CaO-MgO sorbents. The homogeneity of CaO and MgO in the sorbent provided the possibility of high anti-sintering property.

BET specific surface area data of the sorbent precursors were also determined using a nitrogen sorption technique. Figure 3b,c shows the adsorption/desorption isotherms of $Mg_{.064}Ca_{.936}CO_3$ and $Mg_{.129}Ca_{.871}CO_3$. The prepared $Mg_{.064}Ca_{.936}CO_3$ and $Mg_{.129}Ca_{.871}CO_3$ sorbent precursors possess specific surface areas of 98.7 and 53.3 m^2/g. The possible reason may be the effect of PSS during the precipitation, which dispersed Ca^{2+} and Mg^{2+} effectively to form the porous sphere structure, thus gaining a high specific surface area.

The multiple cycles of CO_2 carbonation capacity comparison of three samples was illustrated in Figure 11. As shown in

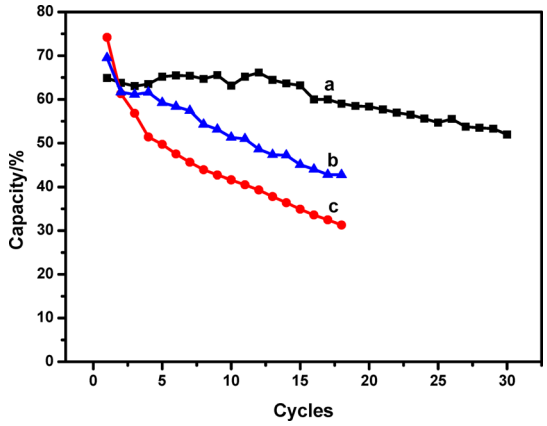

Figure 11. Carbonation capacity vs cycles for sorbents (a) $Mg_{.129}Ca_{.871}CO_3$, (b) $Mg_{.064}Ca_{.936}CO_3$, and (c) $CaCO_3$ precipitation without PSS. Carbonation: 650 °C, 45 min, 50% CO_2 in N_2. Calcination: 700 °C, 30 min, pure N_2.

Figure 11, the CaO-based sorbents derived from $Mg_{.064}Ca_{.936}CO_3$ and $Mg_{.129}Ca_{.871}CO_3$ possessed better stability than pure CaO derived from $CaCO_3$ precipitation without PSS, which was benefited from the inert MgO preventing the sintering of CaO. The initial capacity of sorbent calcinated from $Mg_{.064}Ca_{.936}CO_3$ was 68.9%, lower than 74.2% of pure CaO sorbent due to the decrease of active CaO, however, its stability was better than pure CaO although it also experienced capacity decaying during multiple cycles. On the other hand, the sorbent with higher MgO mass fraction had a relatively lower initial uptake but were more stable over multiple cycles. The carbonation capacity of sorbent derived from $Mg_{.129}Ca_{.871}CO_3$ remained about 52.0% after 30 carbonation/calcination cycles, exhibiting the favorable stability because of the doping with more inert MgO.

The favorable carbonation capacity of the synthetic CaO-MgO sorbents is mainly attributed to the porous structure, which generated a much larger specific surface area and pore volume. And more importantly, the inert support materials (MgO), which are distributed in the sorbent uniformly and separate CaO grains greatly, delayed the sintering of CaO particles at high carbonation and calcination temperatures effectively. Multicycle capacity stability of CaO sorbents has been achieved by the addition of second-phase refractory "-spacer-" particles to inhibit densification of the CaO particle matrix.

CONCLUSIONS

A PSS-assisted fast precipitation synthesis for preparing CaO-based sorbents provides a remarkable development of specific surface area and pore volume compared to those prepared in the absence of PSS. The presence of PSS effectively prevents the agglomeration of the CaO particles and obtains porous sphere structure with the improved specific surface area and pore volume. The favorable capacity of 74.2% was obtained in the initial carbonation cycle. When Ca^{2+} and Mg^{2+} are precipitated simultaneously in the presence of PSS, as a surprising result, the CaO-based sorbents gain the same porous sphere structure and maintain a high specific surface area, resulting in the higher initial carbonation capacity. The stable capacity of about 52.0% was achieved over 30 carbonation/calcination cycles due to the uniform distribution of MgO in

the CaO-based sorbents derived from $Mg_{.129}Ca_{.871}CO_3$, which improves the anti-sintering of the sorbents.

AUTHOR INFORMATION

Corresponding Author

*Shengping Wang. E-mail: spwang@tju.edu.cn.

Notes

The authors declare no competing financial interest.

ACKNOWLEDGMENTS

Financial support by Natural Science Foundation of China (NSFC) (Grant No. 21176179), the Program for New Century Excellent Talents in University (NCET-13-0411), and the Program of Introducing Talents of Discipline to Universities (B06006) is gratefully acknowledged.

REFERENCES

(1) D'Alessandro, D. M.; Smit, B.; Long, J. R. Carbon Dioxide Capture: Prospects for New Materials. *Angew. Chem., Int. Ed.* **2010**, *49*, 6058−6082.

(2) Kierzkowska, A. M.; Pacciani, R.; Mueller, C. R. CaO-based CO_2 Sorbents: From Fundamentals to the Development of New, Highly Effective Materials. *ChemSusChem* **2013**, *6*, 1130−1148.

(3) Wang, S.; Yan, S.; Ma, X.; Gong, J. Recent Advances in Capture of Carbon Dioxide Using Alkali-Metal-based Oxides. *Energy Environ. Sci.* **2011**, *4*, 3805−3819.

(4) Choi, S.; Drese, J. H.; Jones, C. W. Adsorbent Materials for Carbon Dioxide Capture from Large Anthropogenic Point Sources. *ChemSusChem* **2009**, *2*, 796−854.

(5) Sayari, A.; Belmabkhout, Y. Stabilization of Amine-Containing CO_2 Adsorbents: Dramatic Effect of Water Vapor. *J. Am. Chem. Soc.* **2010**, *132*, 6312−6314.

(6) Son, W.-J.; Choi, J.-S.; Ahn, W.-S. Adsorptive Removal of Carbon Dioxide Using Polyethyleneimine-loaded Mesoporous Silica Materials. *Microporous Mesoporous Mater.* **2008**, *113*, 31−40.

(7) Wickramaratne, N. P.; Jaroniec, M. Activated Carbon Spheres for CO_2 Adsorption. *ACS Appl. Mater. Interfaces* **2013**, *5*, 1849−1855.

(8) Jang, H. J.; Lee, C. H.; Kim, S.; Kim, S. H.; Lee, K. B. Hydrothermal Synthesis of K_2CO_3-Promoted Hydrotalcite from Hydroxide-Form Precursors for Novel High-Temperature CO_2 Sorbent. *ACS Appl. Mater. Interfaces* **2014**, *6*, 6914−6919.

(9) Gupta, H.; Fan, L. S. Carbonation-Calcination Cycle Using High Reactivity Calcium Oxide for Carbon Dioxide Separation from Flue Gas. *Ind. Eng. Chem. Res.* **2002**, *41*, 4035−4042.

(10) Dasgupta, D.; Mondal, K.; Wiltowski, T. Robust, High Reactivity and Enhanced Capacity Carbon Dioxide Removal Agents for Hydrogen Production Applications. *Int. J. Hydrogen Energy* **2008**, *33*, 303−311.

(11) Li, L.; King, D. L.; Nie, Z.; Li, X. S.; Howard, C. $MgAl_2O_4$ Spinel-Stabilized Calcium Oxide Absorbents with Improved Durability for High-Temperature CO_2 Capture. *Energy Fuels* **2010**, *24*, 3698−3703.

(12) Manovic, V.; Anthony, E. J. Sintering and Formation of a Nonporous Carbonate Shell at the Surface of CaO-based Sorbent Particles during CO_2-Capture Cycles. *Energy Fuels* **2010**, *24*, 5790−5796.

(13) Liu, W.; Feng, B.; Wu, Y.; Wang, G.; Barry, J.; da Costa, J. C. D. Synthesis of Sintering-Resistant Sorbents for CO_2 Capture. *Environ. Sci. Technol.* **2010**, *44*, 3093−3097.

(14) Zhou, Z.; Qi, Y.; Xie, M.; Cheng, Z.; Yuan, W. Synthesis of CaO-based Sorbents through Incorporation of Alumina/Aluminate and Their CO_2 Capture Performance. *Chem. Eng. Sci.* **2012**, *74*, 172−180.

(15) Zhao, M.; Bilton, M.; Brown, A. P.; Cunliffe, A. M.; Dvininov, E.; Dupont, V.; Comyn, T. P.; Milne, S. J. Durability of $CaO−CaZrO_3$ Sorbents for High-Temperature CO_2 Capture Prepared by a Wet Chemical Method. *Energy Fuels* **2014**, *28*, 1275−1283.

(16) Wang, Y.; Zhu, Y.; Wu, S. A New Nano CaO-based CO_2 Adsorbent Prepared Using an Adsorption Phase Technique. *Chem. Eng. J.* **2013**, *218*, 39−45.

(17) Luo, C.; Zheng, Y.; Yin, J.; Qin, C.; Ding, N.; Zheng, C.; Feng, B. Effect of Support Material on Carbonation and Sulfation of Synthetic CaO-based Sorbents in Calcium Looping Cycle. *Energy Fuels* **2013**, *27*, 4824−4831.

(18) Li, Y.; Zhao, C.; Qu, C.; Duan, L.; Li, Q.; Liang, C. CO_2 Capture using CaO Modified with Ethanol/water Solution during Cyclic Calcination/carbonation. *Chem. Eng. Technol.* **2008**, *31*, 237−244.

(19) Wang, S.; Shen, H.; Fan, S.; Zhao, Y.; Ma, X.; Gong, J. Enhanced CO_2 Adsorption Capacity and Stability using CaO-based Adsorbents Treated by Hydration. *AIChE J.* **2013**, *59*, 3586−3593.

(20) Sun, R.; Li, Y.; Wu, S.; Liu, C.; Liu, H.; Lu, C. Enhancement of CO_2 Capture Capacity by Modifying Limestone with Propionic Acid. *Powder Technol.* **2013**, *233*, 8−14.

(21) Ridha, F. N.; Manovic, V.; Macchi, A.; Anthony, M. A.; Anthony, E. J. Assessment of Limestone Treatment with Organic Acids for CO_2 Capture in Ca-Looping Cycles. *Fuel Process. Technol.* **2013**, *116*, 284−291.

(22) Xu, P.; Xie, M.; Cheng, Z.; Zhou, Z. CO_2 Capture Performance of CaO-based Sorbents Prepared by a Sol−Gel Method. *Ind. Eng. Chem. Res.* **2013**, *52*, 12161−12169.

(23) Luo, C.; Zheng, Y.; Zheng, C.; Yin, J.; Qin, C.; Feng, B. Manufacture of Calcium-based Sorbents for High Temperature Cyclic CO_2 Capture via a Sol−Gel Process. *Int. J. Greenhouse Gas Control* **2013**, *12*, 193−199.

(24) Liu, W.; Yin, J.; Qin, C.; Feng, B.; Xu, M. Synthesis of CaO-based Sorbents for CO_2 Capture by a Spray-Drying Technique. *Environ. Sci. Technol.* **2012**, *46*, 11267−11272.

(25) Sayyah, M.; Lu, Y.; Masel, R. I.; Suslick, K. S. Mechanical Activation of CaO-based Adsorbents for CO_2 Capture. *ChemSusChem* **2013**, *6*, 193−198.

(26) Akgsornpeak, A.; Witoon, T.; Mungcharoen, T.; Limtrakul, J. Development of Synthetic CaO Sorbents via CTAB-Assisted Sol−Gel Method for CO_2 Capture at High Temperature. *Chem. Eng. J.* **2014**, *237*, 189−198.

(27) Yang, Z.; Zhao, M.; Florin, N. H.; Harris, A. T. Synthesis and Characterization of CaO Nanopods for High Temperature CO_2 Capture. *Ind. Eng. Chem. Res.* **2009**, *48*, 10765−10770.

(28) Chen, S. F.; Yu, S. H.; Wang, T. X.; Jiang, J.; Colfen, H.; Hu, B.; Yu, B. Polymer-Directed Formation of Unusual $CaCO_3$ Pancakes with Controlled Surface Structures. *Adv. Mater.* **2005**, *17*, 1461−1465.

(29) Guo, X. H.; Yu, S. H.; Cai, G. B. Crystallization in a Mixture of Solvents by Using a Crystal Modifier: Morphology Control in the Synthesis of Highly Monodisperse $CaCO_3$ Microspheres. *Angew. Chem., Int. Ed.* **2006**, *45*, 3977−3981.

(30) Kim, S.; Ko, J. W.; Park, C. B. Bio-inspired Mineralization of CO_2 Gas to Hollow $CaCO_3$ Microspheres and Bone Hydroxyapatite/Polymer Composites. *J. Mater. Chem.* **2011**, *21*, 11070−11073.

(31) Wang, Y.; Moo, Y. X.; Chen, C.; Gunawan, P.; Xu, R. Fast Precipitation of Uniform $CaCO_3$ Nanospheres and Their Transformation to Hollow Hydroxyapatite Nanospheres. *J. Colloid Interface Sci.* **2010**, *352*, 393−400.

(32) Wang, C.; He, C.; Tong, Z.; Liu, X.; Ren, B.; Zeng, F. Combination of Adsorption by Porous $CaCO_3$ Microparticles and Encapsulation by Polyelectrolyte Multilayer Films for Sustained Drug Delivery. *Int. J. Pharm.* **2006**, *308*, 160−167.

(33) Wang, T. X.; Colfen, H.; Antonietti, M. Nonclassical Crystallization: Mesocrystals and Morphology Change of $CaCO_3$ Crystals in the Presence of a Polyelectrolyte Additive. *J. Am. Chem. Soc.* **2005**, *127*, 3246−3247.

(34) Wang, T.; Antonietti, M.; Colfen, H. Calcite Mesocrystals: "Morphing" Crystals by a Polyelectrolyte. *Chem.—Eur. J.* **2006**, *12*, 5722−5730.